MEaSURES Vegetation Continuous Fields ESDR
Algorithm Theoretical Basis Document (ATBD)

Version 2.0

MEaSURES Vegetation Continuous Fields ESDR
for the AVHRR and MODIS Records: 1982-2016
Principal Investigator:

Matthew Hansen
Department of Geographical Sciences
University of Maryland
College Park, MD

Document Prepared By:

Xiaopeng Song, Charlene DiMiceli, Mark Carroll, Rob Sohlberg, Do-Hyung Kim, John Townshend

Department of Geographical Sciences

Table of Contents

University of Maryland
College Park, MD

January 24, 2018

MEaSURES Vegetation Continuous Fields ESDR
Algorithm Theoretical Basis Document (ATBD)
Version 2.0

1. Introduction

This document describes the methods used to derive global Vegetation Continuous Fields (VCF) Earth Science Data Records (ESDRs). Section 1 discusses the rationale for generating the ESDR. Section 2 provides an overview of the products and technical background information. Section 3 provides details of the methods used to generate the output products. Specifically, it describes the input data, the preprocessing steps used to prepare it, and the methods used for creating training data for supervised model building. It then describes the data mining algorithms and software used to create the regression trees. Finally, it contains a description of the output products, including format, metadata, and error measures.

The following references supply further information about the history and development of VCF products:

Carroll, M. L., John R. Townshend, Charlene M. DiMiceli, Praveen Noojipady, and R. A. Sohlberg. "A new global raster water mask at 250 m resolution." International Journal of Digital Earth 2, no. 4 (2009): 291-308.

DeFries, Ruth, Matthew Hansen, and John Townshend. "Global discrimination of land cover types from metrics derived from AVHRR Pathfinder data." Remote Sensing of Environment 54, no. 3 (1995): 209-222.

DeFries, Ruth, Matthew Hansen, Marc Steininger, Ralph Dubayah, Robert Sohlberg, and John Townshend. "Subpixel forest cover in Central Africa from multisensor, multitemporal data." Remote Sensing of Environment 60, no. 3 (1997): 228-246.

DeFries, R. S., J. R. G. Townshend, and M. C. Hansen. "Continuous fields of vegetation characteristics at the global scale at 1-km resolution." Journal of Geophysical Research: Atmospheres (1984–2012) 104, no. D14 (1999): 16911-16923.

DeFries, R. S., M. C. Hansen, and J. R. G. Townshend. "Global continuous fields of vegetation characteristics: a linear mixture model applied to multi-year 8 km AVHRR data." International Journal of Remote Sensing 21, no. 6-7 (2000): 1389-1414.

Hansen, M. C., R. S. DeFries, John RG Townshend, and Rob Sohlberg. "Global land cover classification at 1 km spatial resolution using a classification tree approach." International Journal of Remote Sensing 21, no. 6-7 (2000): 1331-1364.

Hansen, M. C., R. S. DeFries, J. R. G. Townshend, R. Sohlberg, C. Dimiceli, and M. Carroll. "Towards an operational MODIS continuous field of percent tree cover algorithm: examples using AVHRR and MODIS data." Remote Sensing of Environment 83, no. 1 (2002a): 303-319.

Hansen, M. C., R. S. DeFries, J. R. G. Townshend, L. Marufu, and R. Sohlberg. "Development of a MODIS tree cover validation data set for Western Province, Zambia." Remote Sensing of Environment 83, no. 1 (2002b): 320-335.

Hansen, Matthew C., and Ruth S. DeFries. "Detecting long-term global forest change using continuous fields of tree-cover maps from 8-km Advanced Very High Resolution Radiometer (AVHRR) data for the years 1982–99." Ecosystems 7, no. 7 (2004): 695-716.

Hansen, M. C., P. V. Potapov, R. Moore, M. Hancher, S. A. Turubanova, A. Tyukavina, D. Thau et al. "High-resolution global maps of 21st-century forest cover change." Science 342, no. 6160 (2013): 850-853.

Pedelty, Jeffrey, Sadashiva Devadiga, Edward Masuoka, Molly Brown, Jorge Pinzon, Compton Tucker, D. Roy et al. "Generating a long-term land data record from the AVHRR and MODIS instruments." In Geoscience and Remote Sensing Symposium, 2007. IGARSS 2007. IEEE International, pp. 1021-1025. IEEE, 2007.

Sexton, Joseph O., Xiao-Peng Song, Min Feng, Praveen Noojipady, Anupam Anand, Chengquan Huang, Do-Hyung Kim et al. "Global, 30-m resolution continuous fields of tree cover: Landsat-based rescaling of MODIS vegetation continuous fields with lidar-based estimates of error." International Journal of Digital Earth 6, no. 5 (2013): 427-448.

Song, Xiao-Peng, Chengquan Huang, Min Feng, Joseph O. Sexton, Saurabh Channan, and John R. Townshend. "Integrating global land cover products for improved forest cover characterization: An application in North America." International Journal of Digital Earth ahead-of-print (2013): 1-16.

2. Overview

Vegetation mosaics occur at all spatial scales on the earth's land surface. At the landscape scale, patches of trees, grass, and bare ground are distributed heterogeneously across the land surface. At the local scale, mixtures exist even within plots of several square meters. While boundaries between vegetation types may be fairly abrupt in some locations, such as the boundary between a forest and an alpine meadow at a tree line, gradients in vegetation usually occur gradually across the landscape, with no sharp boundary between types.

Vegetation continuous fields (VCFs) are continuous representations of vegetation canopy cover. For each pixel in a satellite image, percent cover is given for each vegetation category; there are four basic categories in the MEaSUREs ESDR products: tree cover, non-tree vegetation, bare ground, and water. The tree cover layer is subdivided into additional categories: evergreen, deciduous, broadleaf and needleleaf. Figure 1 depicts an example of VCF percent tree cover in the Amazon basin at decadal intervals derived from the Land Long-Term Data Record (LTDR).

Earth science research requires global characterization of vegetation parameters such as fractional cover, biomass, albedo, leaf area index, and photosynthetic capacity. Given the difficulty of making direct measurements of these variables, estimates must be based on remote sensing data. Traditionally, land cover maps divide vegetation cover into discrete ecosystem types; researchers then assign constant vegetation parameters to each type. Deriving vegetation characteristics in this manner has inherent flaws: 1) vegetation density and species composition vary significantly within an ecosystem and are not well represented by a single value; 2) category definitions and boundaries vary from map to map, making them difficult to compare and interpret; 3) parameters change abruptly across ecosystem boundaries; and 4) mixtures of vegetation types are poorly characterized by discrete classifications.

VCFs were developed to overcome these flaws and provide the improved depiction of vegetation cover needed for many applications. The most direct application of VCF products is the quantification of deforestation and forest degradation over time, providing the ability to monitor global forests in a consistent and objective manner [Hansen et al. 2013, Huang et al. 2009]. VCFs are also being used to parameterize climate and land surface models, estimate biomass and fluxes for carbon modeling, and determine anthropogenic land cover change [Tang and Bartlein, 2008; van der Werf, 2006, 2010; Hansen and Defries, 2004; Giglio, *et al.*, 2009]. They provide fundamental base maps for studies of fire risk, ecosystem functioning, and biodiversity.

A number of methods have been used to derive subpixel vegetation cover using remotely sensed data. Early approaches include: (1) fuzzy membership functions [1994; Foody and Cox, 1994]; (2) isolines in red and near infrared scatter plots inferred from geometric models of plant cover [Jasinski, 1996]; (3) empirical relationships derived from high resolution data [DeFries *et al.*, 1997; Iverson *et al.*, 1989, 1994; Zhu and Evans, 1992, 1994]; (4) aggregations of discrete classifications [Mayaux and Lambin, 1997]; and (5) linear mixture modeling [Adams *et al.*, 1995; Bierwirth, 1990; Pech *et al.*, 1986; Quarmby *et al.*, 1992; Settle and Drake, 1993]. There were a number of limitations to these approaches: single-scene analysis did not capture phenological clues; models had only local applicability; algorithms used only one or two bands or indices; models defined linear relationships between bands and vegetation density; and methods depended on human interpretation and tuning.

Over the last 15 years, data mining methods have been developed for VCF production that greatly improve upon these earlier methods. In particular, regression tree model methods have evolved to successfully derive global VCF products using AVHRR, MODIS and Landsat data [Defries *et al*. 1999, Hansen *et al*. 2003, Sexton *et al*. 2013, Hansen *et al*. 2013]. Regression tree models provide a non-linear fit to the data, resulting in more accurate predictions over widely

Figure 1. Time series of VCF tree cover for the Amazon Basin from the MEaSUREs VCF ESDR project. (a) 1990, (b) 2000, (c) 2010. Increasing deforestation can be noted in "arc of deforestation" shown in the lower and right sides of the images.

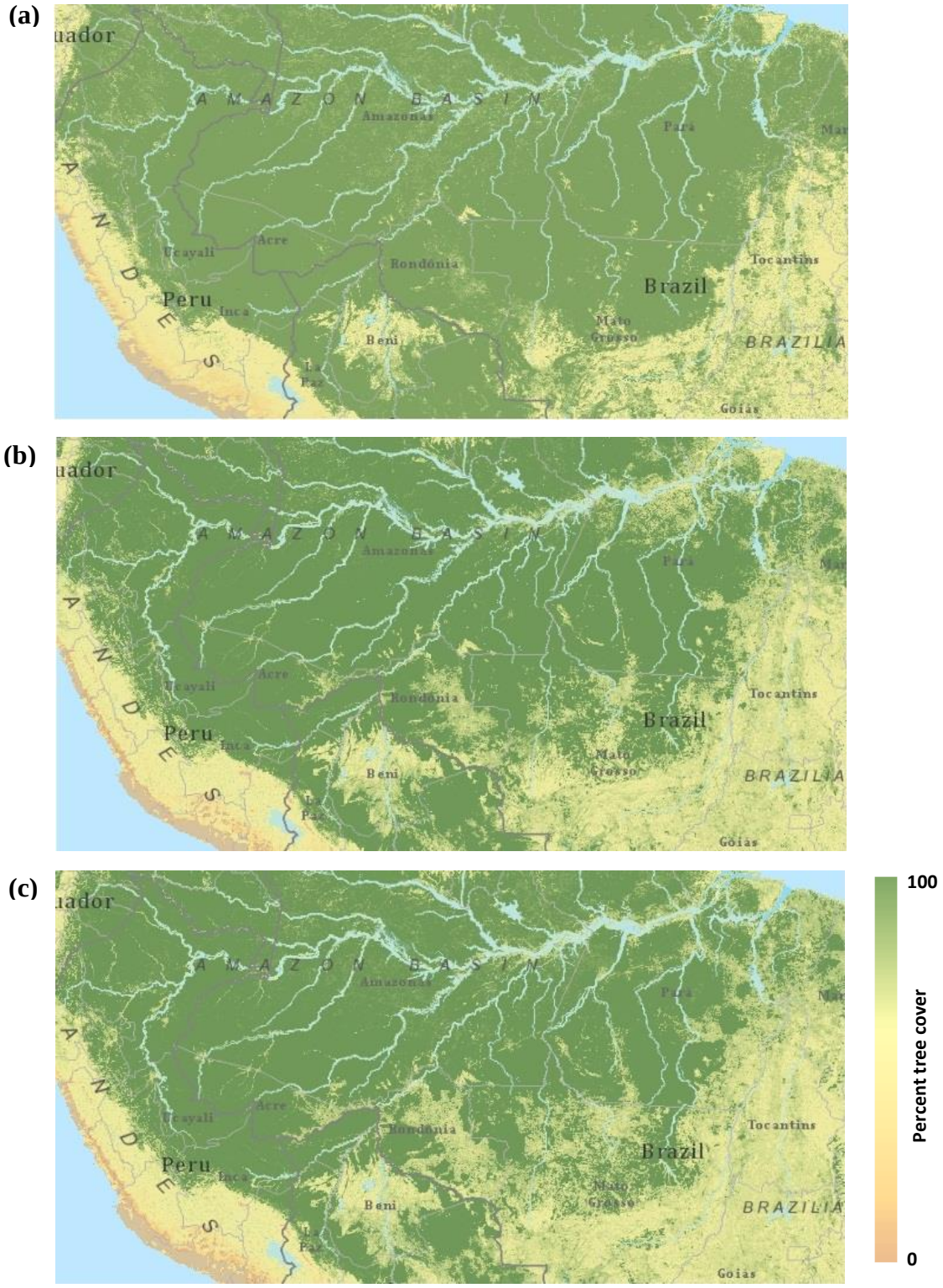

varying land cover types. Increased computer processing power and the availability of robust open source data mining software make it possible to apply these models to the large datasets now available from satellite instruments, in this case, to the LTDR. A further advantage lies in the ability to fully automate the process.

The LTDR data provide a long, consistently-processed time series of surface reflectance, brightness temperature and normalized difference vegetation index (NDVI) from 1981 to the present. This gives us the opportunity to create a corresponding time series of annual VCF products over 30 years for multiple vegetation types, which has not been done before. These products will be of particular importance to the climate and carbon modeling communities, both in benchmarking dynamic vegetation models and as more accurate parameterization of land surface models.

3. MEaSURES VCF ESDR Method

Figure 2 outlines the method used to create the VCF ESDRs. Each step will be discussed in greater detail in the following paragraphs.

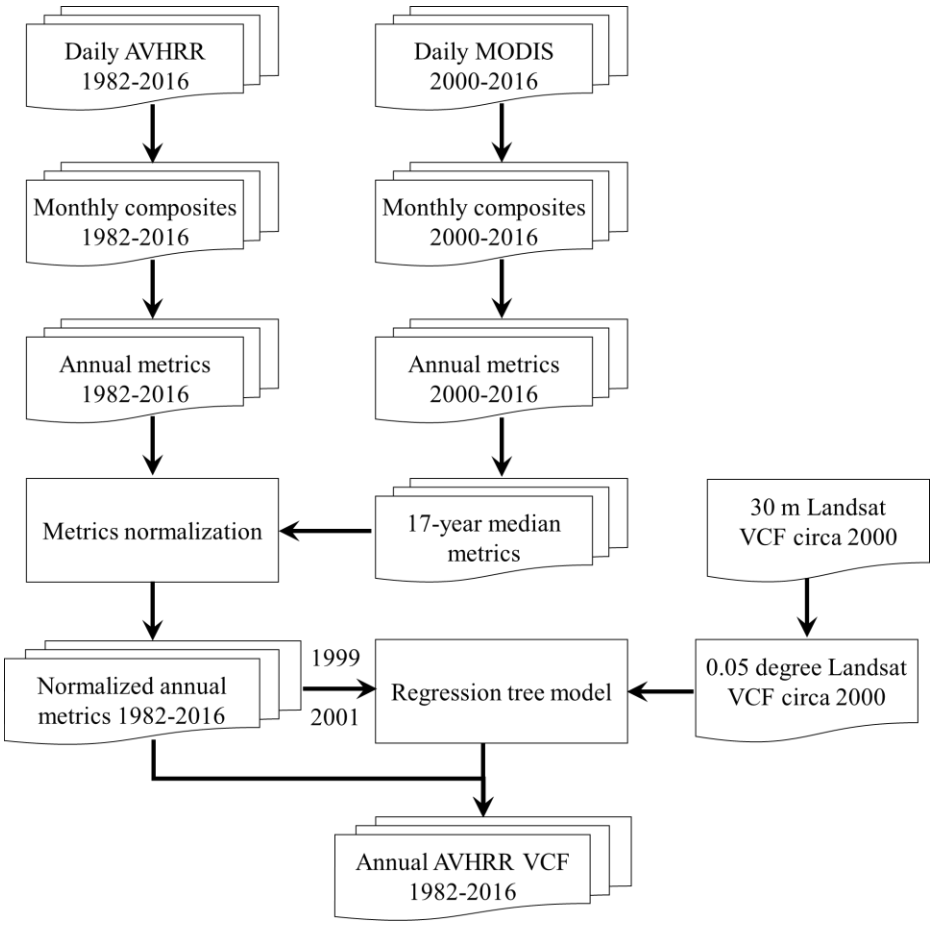

Figure 2. Flowchart of generating the annual AVHRR vegetation continuous fields (VCF) land cover product.

3.1 Definitions

Vegetation continuous fields (VCF) represent land surface as a fractional combination of vegetation functional types that can be remotely sensed from satellites [Defries *et al*., 1995]. Consistent with previous research [DeFries, Townshend, & Hansen 1999; Hansen et al. 2003; Hansen et al. 2002; Hansen et al. 2005; Hansen et al. 2011], the VCF product developed in this study consists of percentages of tree canopy (TC) cover, short vegetation (SV) cover and bare ground (BG) cover. Trees are defined as all vegetation taller than 5 meters in height. TC refers to the proportion of the ground covered by the vertical projection of tree crowns [Jennings, Brown, and Sheil 1999; Korhonen *et al*. 2006]. SV characterizes the proportion of the ground covered by vegetation other than trees, including shrubs, herbaceous vegetation, and mosses, while BG represents the proportion of the land surface not covered by vegetation. Both SV and BG are quantified from nadir view at top of canopy [Ying *et al*. 2017, Hansen *et al*. 2011, Hansen *et al*. 2014]. TC, SV and BG were mapped during the local annual peak of a growing season. TC is not equivalent to forest cover, although forest cover may be defined based on TC. For example, the FAO defines forest as a parcel or unit of land of at least 0.5 hectares in size which is covered by 10% or more trees that are 5 meters or taller [FAO 2015].

3.2 Generation of AVHRR VCF

The Advanced Very High Resolution Radiometer (AVHRR) instruments on-board NOAA satellites remain an important data source for studying long-term changes in land surface properties as they provide the longest time-series of global satellite measurements [Pinzon & Tucker 2014, Tucker *et al*. 2005, Franch *et al*. 2017]. We used the version 4 Long Term Data Record (LTDR) to generate the annual VCF products [Franch *et al*. 2017, Pedelty *et al*. 2007]. The LTDR was compiled from AVHRR observations through a series of processing steps including radiometric calibration, geolocation correction, atmospheric correction and bi-directional reflectance effect correction [Franch *et al*. 2017]. The daily LTDR surface reflectance data contain 5 multi-spectral layers of AVHRR channels 1-5 and the normalized difference vegetation index (NDVI) layer computed from channels 1 and 2 [Tucker 1979]. Each pixel is $0.05° \times 0.05°$ in size. We implemented an improved version of the operational Moderate Resolution Imaging Spectroradiometer Vegetation Continuous Field (MODIS VCF) approach to convert daily LTDR to yearly VCF [Hansen *et al*. 2003].

Daily AVHRR was first aggregated into monthly composites based on the maximum NDVI value in the month. Maximum NDVI composition can minimize cloud contamination, reduce bi-directional and off-nadir viewing effects, minimize band-correlated atmospheric effects and enhance vegetation discrimination [Holben 1986]. The technique has been widely adopted for generating NDVI and land cover products from daily satellite data for sensors such as AVHRR, MODIS and VEGETATION [Tucker 2005, Loveland *et al*. 2000, Hansen *et al*. 2000, Defries *et al*. 1998, Bartholomé 2005].

Monthly composites were subsequently converted to annual phenological metrics [Hansen *et al*. 2013, Hansen *et al*. 2003, Lloyd 1990, Reed 1994, Defries *et al*. 1995]. Metrics are statistical transformations of pixel time-series that can capture the salient features of vegetation phenology while maintaining high spatial and temporal data consistency. Metrics thus provide a unique advantage to large-area land cover mapping and monitoring. We created a total of 735 annual metrics from a combination of 5 multi-spectral bands and one NDVI layer, each available as time-series of 12 months.

An empirical normalization procedure was applied to enhance the year-to-year consistency of the AVHRR metrics. Time-series data from AVHRR are known to have systematic discrepancies due to different satellite platforms, orbital drift, changes in sensor design and sensor degradation [Pinzon & Tucker 2014, Tucker *et al.* 2005, Latifovic *et al.* 2012]. The systematic differences are particularly pronounced before and after year 2000; beginning with NOAA-16 in 2000, satellite orbits were stabilized and a major improvement was introduced in the sensor design to increase sensitivity at the low end of radiance [Pinzon & Tucker 2014]. Research has also shown that the varying observational solar zenith angle as a result of orbital drift affects reflectance more than NDVI and is negatively related to leaf area or positively related to soil exposure [Kaufmann *et al.* 2000]. That is, dense vegetation is less affected than sparse vegetation. Additionally, remaining atmospheric effects in the AVHRR surface reflectance can also cause inconsistency between years. The normalization was designed to remove these artifacts unrelated to actual surface change.

A rich literature exists on calibration of AVHRR time series. One commonly used method is to apply calibration coefficients estimated from "stable targets" such as deserts, oceans, clouds or rainforests [Kaufman & Holben 1993, Vermote & Kaufman 1995, Los 1998, Myneni *et al.* 1998, Gutman 1999, Vermote & Saleous 2006, Donohue *et al.* 2008]. For example, earlier works by Myneni *et al.* [1997, 1998], used the Sahara desert as reference to adjust global NDVI. Gutman [1999] used global deserts and rainforests to correct reflectances as well as NDVI. Recently, data from well-calibrated sensors such as MODIS and SPOT were used as reference for anchoring AVHRR-based NDVI time series [Pinzon & Tucker 2014, Tucker *et al.* 2005].

To normalize annual metrics, we designed a two-step approach, using MODIS data as reference. The first step was to apply a dark object subtraction (DOS) to remove systematic biases for vegetated surfaces, especially forest. DOS is also a simple and effective method of removing atmospheric contamination in remotely sensed data [Hansen *et al.* 2008, Potapov *et al.* 2012, Chavez 1989, Song *et al.* 2001, Woodcock 2001]. We used the intact forest landscapes (IFL) [Potapov *et al.* 2017] of the tropical rainforest biome (i.e. the minimally disturbed tropical rainforests, average tree cover 97%) as the dark stable target, which was also considered a spectral end-member. The second step was to apply a slope-based adjustment for pixels that contain visible bare ground. This step involved the use of tropical, subtropical and temperate deserts with 100% Landsat-based bare ground cover [Ying *et al.* 2017] as the bright stable target, or the other spectral end-member. Biases over other land surfaces are assumed to be within these two extreme end-members [Gutman 1999]. To create the MODIS reference data, an identical procedure was applied to daily MODIS LTDR [Franch *et al.* 2017] to derive annual metrics for years 2000 through 2016. The 17-year median values for each metric were subsequently derived and used as reference.

DOS was conducted by applying the following equations:

$$y_{m,t,i} = x_{m,t,i} - \bar{B}_{m,IFL} \quad (1)$$

$$\bar{B}_{m,IFL} = \frac{\sum_{j=1}^{n_{IFL}} (x_{m,t,j} - r_{m,j})}{n_{IFL}} \quad (2)$$

where, $x_{m,t,i}$ is the original AVHRR value of metric *m* in year *t* and pixel *i*, $y_{m,t,i}$ is the DOS-adjusted AVHRR value, $\bar{B}_{m,IFL}$ is the mean bias of metric *m* over a total of n_{IFL} IFL pixels indexed by *j*, $r_{m,j}$ is the MODIS reference value of metric *m* in IFL pixel *j*.

The soil-induced bias was then corrected relative to the desert end-member, which has maximum residual bias after DOS correction, as well as the IFL end-member, which has minimum residual bias. Dense vegetation is largely immune to this correction. The correction is summarized by the following equations:

$$z_{m,t,i} = y_{m,t,i} - \bar{B}_{m,DES} * \frac{(v_{t,i} - \bar{V}_{t,IFL})}{(\bar{V}_{t,DES} - \bar{V}_{t,IFL})} \quad (3)$$

$$\bar{B}_{m,DES} = \frac{\sum_{k=1}^{n_{DES}} (y_{m,t,k} - r_{m,k})}{n_{DES}} \quad (4)$$

$$\bar{V}_{t,IFL} = \frac{\sum_{j=1}^{n_{IFL}} v_{t,j}}{n_{IFL}} \quad (5)$$

$$\bar{V}_{t,DES} = \frac{\sum_{k=1}^{n_{DES}} v_{t,k}}{n_{DES}} \quad (6)$$

where, $z_{m,t,i}$ is the slope-adjusted AVHRR value of metric *m* in year *t* and pixel *i*, $y_{m,t,i}$ is the DOS-adjusted value from equation (1), $\bar{B}_{m,DES}$ is the mean bias of metric *m* over a total of n_{DES} desert (DES) pixels indexed by *k*, $v_{t,i}$ is the peak growing season NDVI value of pixel *i* in year *t*, $\bar{V}_{t,IFL}$ is the mean peak growing season NDVI value of all IFL pixels, $\bar{V}_{t,DES}$ is the mean peak growing season NDVI value of all desert pixels, and $r_{m,k}$ is the MODIS reference value of metric *m* in desert pixel *k*. Here we use peak growing season NDVI, which is one of the metrics and computed as the mean of all NDVI values between 75 and 100 percentiles, in the slope term instead of the annual mean NDVI as used in Gutman [1999], because our annual VCF represents the vegetation state of the local peak growing season. Using this annual metric (before any correction) dynamically optimizes AVHRR data for the growing season of each year.

Adjusted annual metrics were used as input to supervised regression tree models to generate the annual TC and BG product. This non-parametric machine learning method was chosen as it can accommodate nonlinear relationships between the dependent variable (percent TC or percent BG) and independent variables (AVHRR metrics); in addition, the decision rules are easily interpretable [Hansen *et al.* 1996, Friedl & Brodley 1997, Breiman *et al.* 1984]. Training data for TC were obtained by spatially averaging the circa-2000 Landsat-based percent TC product from 0.00025° × 0.00025° to 0.05° × 0.05°, which was in turn trained using very-high spatial resolution images [Hansen *et al.* 2013]. Likewise, training data for BG were obtained by spatially averaging the circa-2000 Landsat-based percent BG product [Ying *et al.* 2017]. Model training and prediction were performed separately for TC and BG. We pooled two years of AVHRR metrics before and after 2000 (i.e. 1999 and 2001) as input features to train 21 bagged regression tree models to account for the remaining inter-annual bias of AVHRR metrics, if any, as well as to avoid over-fitting of the regression tree algorithm. The 21 trained models were applied to annual AVHRR metrics to generate percent TC and BG for each year. Due to missing data in years 1994 and 2000, TC and BG maps in these two years were not produced from AVHRR, but were linearly interpolated using antecedent and subsequent annual TC or BG

estimates on a per pixel basis. Following the MODIS VCF approach [Hansen *et al.* 2003], annual SV was derived as the residual term by subtracting TC and BG percentages from 100. Permanent water surfaces were excluded based on the Landsat-derived permanent surface water product [Hansen *et al.* 2013].

3.2 Accuracy assessment

The generated TC product was validated against a stratified random sample of TC estimates produced from n = 475 sample blocks distributed across the globe [Pengra *et al.* 2015, Olofsson *et al.* 2012, Stehman *et al.* 2012]. This sample dataset was developed by the United States Geological Survey (USGS). Each sample block was 5-km × 5-km (~0.05° × 0.05°) in size. Sub-meter resolution multi-spectral images including QuickBird, WorldView, IKONOS and GeoEye between years 2002 and 2014, depending on each block, were classified to categorical land cover classes including tree cover [Pengra *et al.* 2015]. The percent TC for each block was computed from these data to provide the reference values for comparison to the AVHRR percent TC. The USGS reference data were developed in Universal Transverse Mercator (UTM) projection and the footprints of the 5-km × 5-km reference sample blocks did not exactly overlap with AVHRR pixels, which were in Geographical Latitude / Longitude projection. This geolocation mismatch inevitably introduced some error in the validation results. Thus, we also evaluated AVHRR TC using the Landsat-based TC estimates. Because the spatial units of the Landsat estimates were spatially aligned with the AVHRR pixels, this comparison is free from geolocation error. For BG and SV, due to the lack of reliable high-resolution reference data, we used Landsat-based BG and SV (computed as 100% – Landsat-based BG% – Landsat-based TC%) estimates at the USGS sample locations as reference data for estimating accuracy. These BG and SV reference data were obtained for the same stratified sample of blocks used to evaluate the AVHRR TC product [Olofsson *et al.* 2012, Stehman *et al.* 2012].

The paired AVHRR and reference VCF values were used to calculate four accuracy metrics including root-mean-square-error (RMSE), mean absolute error (MAE), mean error (ME) and r^2 [Stehman *et al.* 2012, Willmott 1982]:

$$RMSE = \sqrt{\frac{\sum_{i=1}^{n} w_i*(p_i-r_i)^2}{\sum_{i=1}^{n} w_i}} \quad (7)$$

$$MAE = \frac{\sum_{i=1}^{n} w_i*|p_i-r_i|}{\sum_{i=1}^{n} w_i} \quad (8)$$

$$ME = \frac{\sum_{i=1}^{n} w_i*(p_i-r_i)}{\sum_{i=1}^{n} w_i} \quad (9)$$

$$r^2 = 1 - \frac{\sum_{i=1}^{n}(p_i-r_i)^2}{\sum_{i=1}^{n}(p_i-\bar{r})} \quad (10)$$

where p_i, r_i and w_i are estimated VCF, reference VCF and sample weight (inverse of inclusion probability of the sample block for the stratified design) at a location i in a sample of size n; $\bar{r}$ is the estimated mean of the reference values.

We also computed the conventional confusion matrices including overall accuracy (OA), user's accuracy (UA) and producer's accuracy (PA) using the paired AVHRR and reference VCF values and a general ratio estimator [Stehman *et al.* 2012, Cochran 1977]:

$$\hat{R} = \frac{\sum_{h=1}^{H} N_h * \bar{y}_h}{\sum_{h=1}^{H} N_h * \bar{x}_h} \quad (11)$$

Where, H is the total number of strata; N_h is the total number of 5-km × 5-km blocks within stratum h; $\bar{y}_h$ and $\bar{x}_h$ are the sample means of variables y and x in stratum h and the specific identity of y and x depends on the accuracy metric being estimated. To estimate OA, y = area of agreement between AVHRR and reference for a VCF class c in each sample block (i.e. overlapped area) and x = area of the sample block. To estimate UA, y = area of agreement between AVHRR and reference for a VCF class c and x = area of class c mapped by AVHRR. To estimate PA, y = area of agreement between AVHRR and reference for a VCF class c and x = area of class c given by reference.

The estimated variance of $\hat{R}$ is:

$$\hat{V}(\hat{R}) = \frac{1}{\hat{X}^2} \sum_{h=1}^{H} N_h^2 (1 - n_h/N_h)(s_{yh}^2 + \hat{R}^2 * s_{xh}^2 - 2 * \hat{R} * s_{xyh})/n_h \quad (12)$$

where $\hat{X}^2 = \sum_{h=1}^{H} N_h * \bar{x}_h$, n_h is the number of sample blocks selected from population within stratum h, s_{yh}^2 and s_{xh}^2 are the sample variances of y and x for stratum h and s_{xyh} is the sample covariance of the variables of x and y for stratum h. The standard error of $\hat{R}$ is the square root of the estimated variance. As noted above, the identity of x and y depends on the accuracy metric being estimated.

3.3 Description of output files

One VCF ESDR product file is created for each year for tree cover, non-tree vegetation cover and bare ground. Every five years an additional product is produced containing the remaining four layers. The output files are in the geographic projection at 0.05° resolution using the same grid as the Land ESDRs, so these files will overlay. The annual product contains three data layers, a fractional water reference layer, a quality layer and three uncertainty layers corresponding to the three vegetation cover layers, each containing a value for every pixel containing land or inland water:

- Percent tree cover
- Percent non-tree vegetation cover
- Percent bare ground (includes rock, soil, permanent ice and snow, and inland water bodies)
- Percent water reference layer
- Quality flags
- Continuous confidence value layers, one for each cover layer (3 layers total)

The 5-year product contains four data layers, a fractional water reference layer, a quality layer and four uncertainty layers corresponding to the four vegetation cover layers, each containing a value for every pixel containing land or inland water:

- Percent evergreen
- Percent deciduous
- Percent needleleaf
- Percent broadleaf
- Percent water reference layer
- Quality flags
- Continuous confidence value layers, one for each cover layer (4 layers total)

The fractional water layer is derived from the current MODIS land/water map averaged and reprojected to the geographic 0.05° LTDR grid and stored as the fraction of the pixel classified as water. Quality and confidence layers are discussed in the next section.

Layers are stored as scientific datasets (SDS) in the HDF format. We store metadata in the file with version information, information about the input files, projection and file size, and overall quality. Data layers, ancillary layers and metadata are accessible to users through a number of software packages (e.g., ENVI, ArcGIS, PCI Geomatica, GDAL).

NOTE MEaSURES VCF version 1.0 has only 3 data layers and is distributed as a GeoTIFF. Future versions will contain additional data layers (evergreen/deciduous tree cover, broadleaf/needleleaf tree cover) and quality layers.

Data from years 1981, 1985, 1994, and 2000 were excluded due to lack of data in the Long Term Data Record (LTDR) v4.

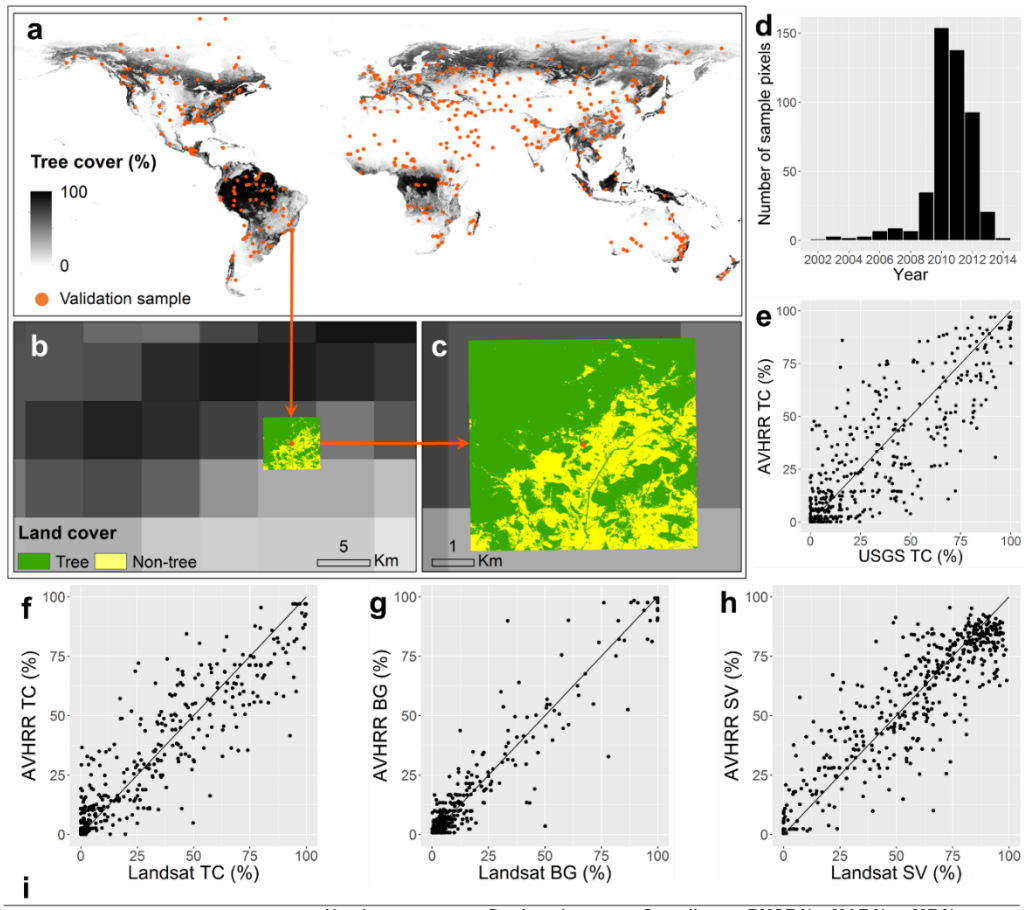

i

Products	Class	User's accuracy % (SE)	Producer's accuracy % (SE)	Overall accuracy % (SE)	RMSE % (SE)	MAE % (SE)	ME % (SE)	r^2
AVHRR TC vs USGS TC	TC	84 (2)	79 (1)	90.1 (0.6)	15.6 (5.0)	9.9 (0.6)	-1.5 (0.8)	0.73
	Not TC	92 (1)	94 (1)					
AVHRR TC vs Landsat TC	TC	85 (1)	88 (1)	93.4 (0.4)	11.2 (3.9)	6.6 (0.4)	1.0 (0.5)	0.85
	Not TC	96 (1)	95 (1)					
AVHRR BG vs Landsat BG	BG	91 (2)	92 (1)	95.6 (0.5)	9.1 (5.1)	4.4 (0.5)	0.4 (0.7)	0.93
	Not BG	97 (1)	97 (1)					
AVHRR SV vs Landsat SV	SV	91 (1)	90 (1)	90.4 (0.6)	14.0 (5.4)	9.6 (0.6)	-0.5 (0.8)	0.79
	Not SV	90 (1)	91 (1)					

Figure 3. Accuracy assessment of AVHRR tree canopy (TC) cover, bare ground (BG) cover and short vegetation (SV) cover, based on a validation sample of 475 AVHRR pixels. (**a)** Spatial distribution of the validation sample (red dot) overlaid on long-term (1982-2016) mean tree cover. The USGS tree cover reference data (5-km × 5-km, Universal Transverse Mercator projection) have greater spatial details (colored squares in **b** and **c**) due to their sub-meter resolution but have geolocation mismatch with the AVHRR product (0.05° × 0.05°, gray-scale squares in **b** and **c**) due to different projections. (**d)** Temporal distribution of the USGS tree cover sample. (e) Scatter plots of AVHRR tree cover against USGS reference tree cover. AVHRR and reference are matched by year and center coordinates. (**f-h)** Scatter plots of AVHRR TC, BG and SV (year 2001) against Landsat-based estimates, which are free from geolocation mismatch. (**i)** Quantitative error metrics, including conventional confusion matrices as well as root-mean-square-error (RMSE), mean absolute error (MAE), mean error (ME) and r^2. The standard error (SE) for the estimated error metrics is provided in the parentheses.

4. References

Adams, John B., Donald E. Sabol, Valerie Kapos, Raimundo Almeida Filho, Dar A. Roberts, Milton O. Smith, and Alan R. Gillespie. "Classification of multispectral images based on fractions of endmembers: Application to land-cover change in the Brazilian Amazon." Remote sensing of Environment 52, no. 2 (1995): 137-154.

Bartholomé, E. & Belward, A. S. GLC2000: A new approach to global land cover mapping from Earth observation data. Int. J. Remote Sens. 26, 1959-1977 (2005).

Bierwirth, P. N. "Mineral mapping and vegetation removal via data-calibrated pixel unmixing, using multispectral images." International Journal of Remote Sensing 11, no. 11 (1990): 1999-2017.

Breiman, L., Friedman, J. H., Olshen, R. A. & Stone, C. J. Classification and regression trees. (Chapman & Hall/CRC, 1984).

Chavez Jr, P. S. Radiometric calibration of Landsat Thematic Mapper multispectral images. Photogramm. Eng. Remote Sensing 55, 1285-1294 (1989).

Cochran, W. G. Sampling Techniques (3rd edition). (John Wiley & Sons, 1977).

DeFries, R. S. et al. Mapping the land surface for global atmosphere-biosphere models: Toward continuous distributions of vegetation's functional properties. J. Geophys. Res. 100, 20867-20882 (1995).

DeFries, R. S., Hansen, M., Townshend, J. R. G. & Sohlberg, R. Global land cover classifications at 8 km spatial resolution: The use of training data derived from Landsat imagery in decision tree classifiers. Int. J. Remote Sens. 19, 3141-3168 (1998).

DeFries, R. S., Townshend, J. R. G. & Hansen, M. C. Continuous fields of vegetation characteristics at the global scale at 1-km resolution. J. Geophys. Res. 104, 16911-16923 (1999).

DeFries, R., Hansen, M. & Townshend, J. Global discrimination of land cover types from metrics derived from AVHRR pathfinder data. Remote Sens. Environ. 54, 209-222 (1995).

DeFries, Ruth, Matthew Hansen, Marc Steininger, Ralph Dubayah, Robert Sohlberg, and John Townshend. "Subpixel forest cover in Central Africa from multisensor, multitemporal data." Remote Sensing of Environment 60, no. 3 (1997): 228-246.

Donohue, R. J., Roderick, M. L. & McVicar, T. R. Deriving consistent long-term vegetation information from AVHRR reflectance data using a cover-triangle-based framework. Remote Sens. Environ. 112, 2938-2949 (2008).

FAO. Global Forest Resources Assessment 2015. (UN Food and Agriculture Organization, Rome, Italy, 2015).

Foody, G. M., and D. P. Cox. "Sub-pixel land cover composition estimation using a linear mixture model and fuzzy membership functions." Remote sensing 15, no. 3 (1994): 619-631.

Franch, B. et al. A 30+ year AVHRR land surface reflectance climate data record and its application to wheat yield monitoring. Remote Sens. 9, 296 (2017).

Friedl, M. A. & Brodley, C. E. Decision tree classification of land cover from remotely sensed data. Remote Sens. Environ. 61, 399–409 (1997).

Giglio, Louis, Tatiana Loboda, David P. Roy, Brad Quayle, and Christopher O. Justice. "An active-fire based burned area mapping algorithm for the MODIS sensor." Remote Sensing of Environment 113, no. 2 (2009): 408-420.

Gutman, G. G. On the use of long-term global data of land reflectances and vegetation indices derived from the advanced very high resolution radiometer. J. Geophys. Res. Atmos. 104, 6241-6255 (1999).

Hansen, M. C. et al. A method for integrating MODIS and Landsat data for systematic monitoring of forest cover and change in the Congo basin. Remote Sens. Environ. 112, 2495-2513 (2008).

Hansen, M. C. et al. Continuous fields of land cover for the conterminous United States using Landsat data: First results from the Web-Enabled Landsat Data (WELD) project. Remote Sens. Lett. 2, 279-288 (2011).

Hansen, M. C. et al. Global percent tree cover at a spatial resolution of 500 meters: First results of the MODIS vegetation continuous fields algorithm. Earth Interact. 7, 10 (2003).

Hansen, M. C. et al. High-resolution global maps of 21st-centry forest cover change. Science 342, 850-853 (2013).

Hansen, M. C. et al. Monitoring conterminous United States (CONUS) land cover change with web-enabled Landsat data (WELD). Remote Sens. Environ. 140, 466-484 (2014).

Hansen, M. C. et al. Towards an operational MODIS continuous field of percent tree cover algorithm: examples using AVHRR and MODIS data. Remote Sens. Environ. 83, 303-319 (2002).

Hansen, M. C., DeFries, R. S., Townshend, J. R. G. & Sohlberg, R. A. Global land cover classification at 1 km spatial resolution using a classification tree approach. Int. J. Remote Sens. 21, 1331-1364 (2000).

Hansen, M. C., Townshend, J. R. G., DeFries, R. S. & Carroll, M. Estimation of tree cover using MODIS data at global, continental and regional/local scales. Int. J. Remote Sens. 26, 4359-4380 (2005).

Hansen, M., Dubayah, R. & Defries, R. Classification trees: An alternative to traditional land cover classifiers. Remote Sens. Lett. 17, 1075-1081 (1996).

Holben, B. N. Characteristics of maximum-value composite images from temporal AVHRR data. Int. J. Remote Sens. 7, 1417-1434 (1986).

Iverson, Louis R., Elizabeth A. Cook, and Robin L. Graham. "Regional forest cover estimation via remote sensing: the calibration center concept." Landscape Ecology 9, no. 3 (1994): 159-174.

Iverson, Louis R., Robin Lambert Graham, and Elizabeth A. Cook. "Applications of satellite remote sensing to forested ecosystems." Landscape ecology 3, no. 2 (1989): 131-143.

Jasinski, Michael F. "Estimation of subpixel vegetation density of natural regions using satellite multispectral imagery." *Geoscience and Remote Sensing, IEEE Transactions on* 34, no. 3 (1996): 804-813.

Jennings, S. B., Brown, N. D. & Sheil, D. Assessing forest canopies and understorey illumination: Canopy closure, canopy cover and other measures. Forestry 72, 59-74 (1999).

Kaufman, Y. J. & Holben, B. N. Calibration of the AVHRR visible and near-IR bands by atmospheric scattering, ocean glint and desert reflection. Int. J. Remote Sens. 14, 21-52 (1993).

Kaufmann, R. K. et al. Effect of orbital drift and sensor changes on the time series of AVHRR vegetation index data. IEEE Trans. Geosci. Remote Sens. 38, 2584-2597 (2000).

Korhonen, L., Korhonen, K. T., Rautiainen, M. & Stenberg, P. Estimation of forest canopy cover: A comparison of field measurement techniques. Silva Fenn. 40, 577-588 (2006).

Latifovic, R., Pouliot, D. & Dillabaugh, C. Identification and correction of systematic error in NOAA AVHRR long-term satellite data record. Remote Sens. Environ. 127, 84-97 (2012).

Lloyd, D. A phenological classification of terrestrial vegetation cover using shortwave vegetation index imagery. Int. J. Remote Sens. 11, 2269-2279 (1990).

Los, S. O. Estimation of the ratio of sensor degradation between NOAA AVHRR channels 1 and 2 from monthly NDVI composites. IEEE Trans. Geosci. Remote Sens. 36, 206-213 (1998).

Loveland, T. R. et al. Development of a global land cover characteristics database and IGBP DISCover from 1 km AVHRR data. Int. J. Remote Sens. 21, 1303-1330 (2000).

Mayaux, Philippe, and Eric F. Lambin. "Tropical forest area measured from global land-cover classifications: inverse calibration models based on spatial textures." Remote Sensing of Environment 59, no. 1 (1997): 29-43.

Myneni, R. B., Keeling, C. D., Tucker, C. J., Asrar, G. & Nemani, R. R. Increased plant growth in the northern high latitudes from 1981 to 1991. Nature 386, 698-702 (1997).

Myneni, R. B., Tucker, C. J., Asrar, G. & Keeling, C. D. Interannual variations in satellite-sensed vegetation index data from 1981 to 1991. J. Geophys. Res. Atmos. 103, 6145-6160 (1998).

Olofsson, P. et al. A global land-cover validation data set, part I: Fundamental design principles. Int. J. Remote Sens. 33, 5768-5788 (2012).

Pech, Roger P., R. D. Graetz, and A. W. Davis. "Reflectance modelling and the derivation of vegetation indices for an Australian semi-arid shrubland." International Journal of Remote Sensing 7, no. 3 (1986): 389-403.

Pedelty, J. et al. Generating a long-term land data record from the AVHRR and MODIS Instruments. IEEE Int. Geosci. Remote Sens. Symp. Proc., 1021-1025 (2007).

Pedelty, Jeffrey, Sadashiva Devadiga, Edward Masuoka, Molly Brown, Jorge Pinzon, Compton Tucker, D. Roy et al. "Generating a long-term land data record from the AVHRR and MODIS instruments." In Geoscience and Remote Sensing Symposium, 2007. IGARSS 2007. IEEE International, pp. 1021-1025. IEEE, 2007.

Pengra, B., Long, J., Dahal, D., Stehman, S. V. & Loveland, T. R. A global reference database from very high resolution commercial satellite data and methodology for application to Landsat derived 30m continuous field tree cover data. Remote Sens. Environ. 165, 234-248 (2015).

Pinzon, J. & Tucker, C. A non-stationary 1981–2012 AVHRR NDVI3g time series. Remote Sens. 6, 6929-6960 (2014).

Potapov, P. et al. The last frontiers of wilderness: Tracking loss of intact forest landscapes from 2000 to 2013. Sci. Adv. 3, e1600821 (2017).

Potapov, P. V. et al. Quantifying forest cover loss in Democratic Republic of the Congo, 2000–2010, with Landsat ETM+ data. Remote Sens. Environ. 122, 106-116 (2012).

Quarmby, N. A., J. R. G. Townshend, J. J. Settle, K. H. White, M. Milnes, T. L. Hindle, and N. Silleos. "Linear mixture modelling applied to AVHRR data for crop area estimation." International Journal of Remote Sensing 13, no. 3 (1992): 415-425.

Reed, B. C. et al. Measuring phenological variability from satellite imagery. J. Veg. Sci. 5, 703-714 (1994).

Settle, J. J., and N. A. Drake. "Linear mixing and the estimation of ground cover proportions." International Journal of Remote Sensing 14, no. 6 (1993): 1159-1177.

Sexton, Joseph O., Xiao-Peng Song, Min Feng, Praveen Noojipady, Anupam Anand, Chengquan Huang, Do-Hyung Kim et al. "Global, 30-m resolution continuous fields of tree cover: Landsat-based rescaling of MODIS vegetation continuous fields with lidar-based estimates of error." International Journal of Digital Earth 6, no. 5 (2013): 427-448.

Stehman, S. V., Olofsson, P., Woodcock, C. E., Herold, M. & Friedl, M. A. A global land-cover validation data set, II: Augmenting a stratified sampling design to estimate accuracy by region and land-cover class. Int. J. Remote Sens. 33, 6975-6993 (2012).

Tang, Guoping, and Patrick J. Bartlein. "Simulating the climatic effects on vegetation: approaches, issues and challenges." Progress in Physical Geography 32, no. 5 (2008): 543-556.

Tucker, C. et al. An extended AVHRR 8-km NDVI dataset compatible with MODIS and SPOT vegetation NDVI data. Int. J. Remote Sens. 26, 4485-4498 (2005).

Tucker, C. J. Red and photographic infrared linear combinations for monitoring vegetation. Remote Sens. Environ. 8, 127-150 (1979).

van der Werf, Guido R., James T. Randerson, Louis Giglio, G. J. Collatz, M. Mu, Prasad S. Kasibhatla, Douglas C. Morton, R. S. DeFries, Y. van Jin, and Thijs T. van Leeuwen. "Global fire emissions and the contribution of deforestation, savanna, forest, agricultural, and peat fires (1997–2009)." Atmospheric Chemistry and Physics 10, no. 23 (2010): 11707-11735.

van der Werf, Guido R., James T. Randerson, Louis Giglio, G. James Collatz, Prasad S. Kasibhatla, and A. F. Arellano Jr. "Interannual variability in global biomass burning emissions from 1997 to 2004." Atmospheric Chemistry and Physics 6, no. 11 (2006): 3423-3441.

Vermote, E. & Kaufman, Y. J. Absolute calibration of AVHRR visible and near-infrared channels using ocean and cloud views. Int. J. Remote Sens. 16, 2317-2340 (1995).

Vermote, E. F. & Saleous, N. Z. Calibration of NOAA16 AVHRR over a desert site using MODIS data. Remote Sens. Environ. 105, 214-220 (2006).

Vermote, E., and Y. J. Kaufman. "Absolute calibration of AVHRR visible and near-infrared channels using ocean and cloud views." International Journal of Remote Sensing 16, no. 13 (1995): 2317-2340.

Willmott, C. J. Some comments on the evaluation of model performance. Bull. Am. Meteorol. Soc. 63, 1309-1313 (1982).

Woodcock, C. E., Macomber, S. A., Pax-Lenney, M. & Cohen, W. B. Monitoring large areas for forest change using Landsat: Generalization across space, time and Landsat sensors. Remote Sens. Environ. 78, 194-203 (2001).

Ying, Q. et al. Global bare ground gain from 2000 to 2012 using Landsat imagery. Remote Sens. Environ. 194, 161-176 (2017).

Zhu, Zhiliang, and David L. Evans. "Mapping midsouth forest distributions." Journal of Forestry (1992).

Zhu, Zhiliang, and David L. Evans. "US forest types and predicted percent forest cover from AVHRR data." Photogrammetric engineering and remote sensing 60, no. 5 (1994): 525-531.